

Novel Ways to Probe the Universe with Gamma-Ray Bursts and Quasars

Abraham Loeb

Astronomy Department, Harvard University
Cambridge, MA 02138, USA

Abstract. I consider novel ways by which Gamma-Ray Bursts (GRBs) and quasars can be used to probe the universe. Clues about how and when was the intergalactic medium ionized can be read off the UV emission spectrum of GRB explosions from the first generation of stars. The existence of intergalactic and galactic stars can be inferred from their gravitational microlensing effect on GRB afterglows. Prior to reionization, quasars should be surrounded by a halo of scattered Ly α radiation which probes the neutral intergalactic medium (IGM) around them. The situation is analogous to the appearance of a halo of scattered light around a street lamp which is embedded in a dense fog. Outflows from quasars magnetize the IGM at all redshifts. As a result, the shocks produced by converging flows during the formation of large scale structure in the IGM, accelerate electrons to relativistic energies and become visible in the radio regime through their synchrotron emission and in the γ -ray regime through their inverse-Compton scattering of the microwave background photons. During transient episodes of strong mergers, X-ray clusters should therefore appear as extended radio or γ -ray sources on the sky.

1 Novel Cosmological Studies with Gamma-Ray Bursts

1.1 Preface

Since their discovery four decades ago, quasars have been used as powerful light-houses which probe the intervening universe out to high redshifts, $z \sim 6$ [42,20]. The spectra of almost all quasars show strong emission lines of metals, indicating super-solar enrichment of the emitting gas [40]. This implies that at least in the cores of galaxies, formation of massive stars and their evolution to supernovae preceded the observed quasar activity. If Gamma-Ray Bursts (GRBs) originate from the remnants of massive stars (such as neutron stars or black holes), as seems likely based on recent estimates of their energy output [89,24,23], then they should exist at least out to the same redshift as quasars. Although GRBs are transient events, their peak optical-UV flux can be as bright as that of quasars. Hence, GRBs promise to be as useful as quasars in probing the high-redshift universe.

Not much is known observationally about the universe in the redshift interval $z = 6-30$, when the first generation of galaxies condensed out of the primordial gas left over from the Big Bang (see reviews [3] and [56]). Observations of the microwave background anisotropies indicate that the cosmic gas became neutral at $z \sim 1000$ and remained so at least down to $z \sim 30$ (see, e.g. [87]). On the

other hand, the existence of transmitted flux shortward of the Ly α resonance in the spectrum of the highest-redshift quasars and galaxies (see, for example, Figure 1), indicates that the intergalactic medium was reionized to a level better than 99.9999% by a redshift $z \sim 6$. This follows from the fact that the Ly α optical depth of the intergalactic medium at high-redshifts ($z \gg 1$) is [38],

$$\tau_\alpha = \frac{\pi e^2 f_\alpha \lambda_\alpha n_{HI}(z)}{m_e c H(z)} \approx 6.15 \times 10^5 x_{HI} \left(\frac{\Omega_b h}{0.03} \right) \left(\frac{\Omega_m}{0.3} \right)^{-1/2} \left(\frac{1+z}{10} \right)^{3/2}, \quad (1)$$

where $H \approx 100h \text{ km s}^{-1} \text{ Mpc}^{-1} \Omega_m^{1/2} (1+z)^{3/2}$ is the Hubble parameter at the source redshift z , $f_\alpha = 0.4162$ and $\lambda_\alpha = 1216\text{\AA}$ are the oscillator strength and the wavelength of the Ly α transition; $n_{HI}(z)$ is the average intergalactic density of neutral hydrogen at the source redshift (assuming primordial abundances); Ω_m and Ω_b are the present-day density parameters of all matter and of baryons, respectively; and x_{HI} is the average fraction of neutral hydrogen. Modeling [20] of the *transmitted flux* in Figure 1 implies $\tau_\alpha < 0.5$ or $x_{HI} < 10^{-6}$, i.e., most of the low-density gas throughout the universe is ionized to a level of 99.9999% at $z < 6$. However, there are some dark intervals in the spectrum which could be indicative of regions with a higher neutral fraction [14]. In fact, Becker et al. [4] reported the detection of an extended ($> 300\text{\AA}$ long) dark interval just shortward of the Ly α emission line in the spectrum of the newly discovered quasar SDSS 1030+0524 at $z = 6.28$. The suppression of the flux by a factor > 150 may indicate the first detection of the Gunn-Peterson trough, although caution is warranted since the inferred optical depth $\tau_\alpha > 5$ can be produced by a neutral fraction as small as $X_{HI} \sim 2 \times 10^{-4}$ according to equation (1).

The question: *how and when was the universe reionized?* defines a new frontier in observational cosmology [56]. The UV spectrum of GRB afterglows can be used to probe the ionization and thermal state of the intergalactic gas during the epoch of reionization, at redshifts $z \sim 7\text{--}10$ [64]. The stretching of the temporal evolution of GRB lightcurves by the cosmological redshift factor $(1+z)$, makes it easier for an observer to react in time and measure a spectrum of their optical-UV emission at its peak.

Energy arguments suggest that reionization resulted from photoionization and not from collisional ionization [81,28]. The corresponding sources of UV photons were either stars or quasars. Recent simulations of the first generation of stars that formed out of the primordial metal-free gas indicate that these stars were likely massive [9,1]. If GRBs result from compact stellar remnants, such as black holes or neutron stars, then the fraction of all stars that lead to GRBs may have been higher at early cosmic times. This, however, is true only if the GRB phenomena is triggered on a time scale much shorter than the age of the universe at the corresponding redshift, which for $z \gg 1$ is $\sim 5.4 \times 10^8 \text{ yr } (h/0.7)^{-1} (\Omega_m/0.3)^{-1/2} [(1+z)/10]^{-3/2}$.

1.2 Properties of High-Redshift GRB Afterglows

Young (days to weeks old) GRBs outshine their host galaxies in the optical regime. In the standard hierarchical model of galaxy formation, the character-

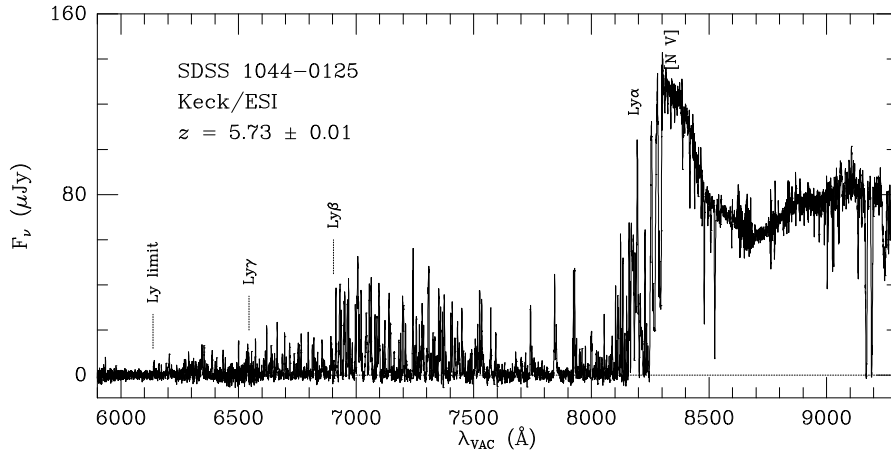


Fig. 1. Spectrum of the quasar SDSS1044-0125 at $z = 5.73$ (Djorgovski et al. 2001), originally discovered by the Sloan Digital Sky Survey (Fan et al. 2000).

istic mass and hence optical luminosity of galaxies and quasars declines with increasing redshift [39,79,3]. Hence, GRBs should become easier to observe than galaxies or quasars at increasing redshift. Similarly to quasars, GRB afterglows possess broad-band spectra which extend into the rest-frame UV and can probe the ionization state and metallicity of the IGM out to the epoch when it was reionized at redshifts $z \sim 7-10$ [56]. Lamb & Reichart [54] have extrapolated the observed γ -ray and afterglow spectra of known GRBs to high redshifts and emphasized the important role that their detection might play in probing the IGM. Simple scaling of the long-wavelength spectra and temporal evolution of afterglows with redshift implies that at a fixed time lag after the GRB trigger in the observer's frame, there is only a mild change in the *observed* flux at infrared or radio wavelengths as the GRB redshift increases. Ciardi & Loeb [12] demonstrated this behavior using a detailed extrapolation of the GRB fireball solution into the non-relativistic regime (see the $2\mu\text{m}$ curves in Figure 2). Despite the strong increase of the luminosity distance with redshift, the observed flux for a given observed age is almost independent of redshift in part because of the special spectrum of GRB afterglows (see Figure 4), but mainly because afterglows are brighter at earlier times and a given observed time refers to an earlier intrinsic time in the source frame as the source redshift increases. The mild dependence of the long-wavelength ($\lambda_{\text{obs}} > 1\mu\text{m}$) flux on redshift stands in contrast to other high-redshift sources such as galaxies or quasars, which fade rapidly with increasing redshift [39,79,3]. Hence, GRBs provide exceptional lighthouses for probing the universe at $z = 6-30$, at the epoch when the first stars had formed.

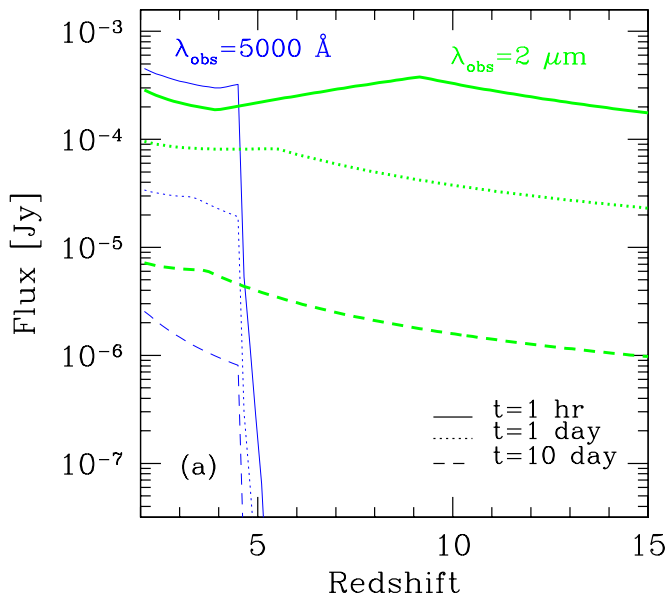


Fig. 2. Theoretical expectation for the observed afterglow flux of a GRB as a function of its redshift (from Ciardi & Loeb 2000). The curves refer to an observed wavelength of 5000 Å (thin lines) and 2 μ m (thick lines). Different line types refer to different observed times after the GRB trigger, namely 1 hour (solid line), 1 day (dotted) and 10 days (dashed). The 5000 Å flux is strongly absorbed at $z > 4.5$ by intergalactic hydrogen. However, at infrared and radio wavelengths the observed afterglow flux shows only a mild dependence on the source redshift.

Assuming that the GRB rate is proportional to the star formation rate and that the characteristic energy output of GRBs is $\sim 10^{52}$ ergs, Ciardi & Loeb [12] predicted that there are always ~ 15 GRBs from redshifts $z > 5$ across the sky which are brighter than ~ 100 nJy at an observed wavelength of $\sim 2 \mu$ m. The infrared spectrum of these sources could be taken with future telescopes such as the *Next Generation Space Telescope* (planned for launch in 2009; see <http://ngst.gsfc.nasa.gov/>), as a follow-up on their early X-ray localization with the *Swift* satellite (planned for launch in 2003; see <http://swift.sonoma.edu/>).

The redshifts of GRB afterglows can be estimated photometrically from either the Lyman limit or Ly α troughs in their spectra. At low redshifts, the question of whether the Lyman limit or Ly α trough interpretation applies depends on the absorption properties of the host galaxy. If the GRB originates from within the disk of a star-forming galaxy, then the afterglow spectrum will likely show a damped Ly α trough. At $z > 6$ the Ly α trough would inevitably exist since the intergalactic Ly α opacity is $> 90\%$ (see Figure 13 in [79]). Interestingly, an absorption feature in the afterglow spectrum which is due to the neutral hydrogen within a molecular cloud or the disk of the host galaxy, is likely

to be time-dependent due to the ionization caused by the UV illumination of the afterglow itself along the line-of-sight [69].

So far, there have been two claims for high-redshift GRBs. Fruchter [25] argued that the photometry of GRB 980329 is consistent with a Ly α trough due to IGM absorption at $z \sim 5$. Anderson et al. [2] inferred a redshift of $z = 4.5$ for GRB 000131 based on a crude optical spectrum that was taken by the VLT a few days after the GRB trigger. *These cases emphasize the need for a coordinated observing program that will alert 10-meter class telescopes to take a spectrum of an afterglow about a day after the GRB trigger, based on a photometric assessment (obtained with a smaller telescope using the Lyman limit or Ly α troughs) that the GRB may have originated at a high redshift.*

In the following two subsections, I illustrate the usefulness of GRB afterglows for cosmological studies through two examples.

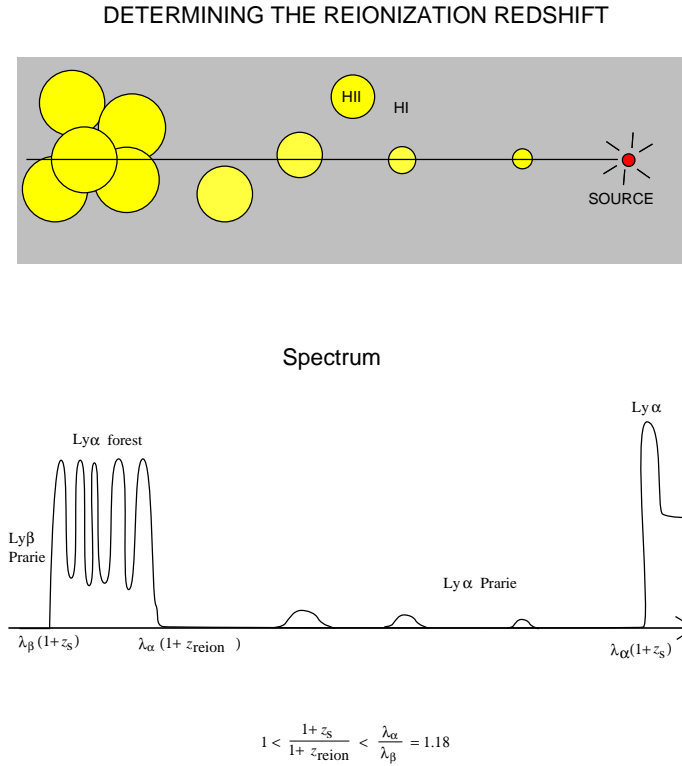


Fig. 3. Sketch of the expected spectrum of a source at a redshift z_s slightly above the reionization redshift z_{reion} . The transmitted flux due to HII bubbles in the pre-reionization era, and the Ly α forest in the post-reionization era, are exaggerated for illustration.

1.3 Probing the Reionization Epoch and Metallicity History of the IGM

The UV spectra of GRB afterglows can be used to measure the evolution of the neutral intergalactic hydrogen with redshift. Figure 3 illustrates schematically the expected absorption just beyond the reionization redshift. Resonant scattering suppresses the spectrum at all wavelengths corresponding to the Ly α resonance prior to reionization. Since the Ly α cross-section is very large, any transmitted flux prior to reionization reflects a large volume of ionized hydrogen along the line-of-sight. If the GRB is located at a redshift larger by $> 18\%$ than the reionization redshift, then the Ly α and the Ly β troughs will overlap. Unlike quasars, GRBs do not ionize the IGM around them; their limited energy supply $\sim 10^{52}$ ergs [89,24,23] can ionize only $\sim 4 \times 10^5 M_\odot$ of neutral hydrogen within their host galaxy.

Quasar spectra indicate the existence of an IGM metallicity which is a fraction of a percent of the solar value [17]. The metals were likely dispersed into the IGM through outflows from galaxies, driven by either supernova or quasar winds [3,28]. Detection of metal absorption lines in the spectrum of GRB afterglows, produced either in the IGM or the host galaxy of the GRB, can help unravel the evolution of the IGM metallicity with redshift and its link to the evolution of galaxies. Detection of X-ray absorption by intergalactic metals can be used to establish the existence of the warm component of the IGM which has not been observed so far [22,43,69].

1.4 Cosmological Microlensing of Gamma-Ray Bursts

Loeb & Perna [57] noted the coincidence between the angular size of a solar-mass lens at a cosmological distance and the micro-arcsecond size of the image of a GRB afterglow. They therefore suggested that microlensing by stars can be used to resolve the photospheres of GRB fireballs at cosmological distances. (Alternative methods, such as radio scintillations, only provide a constraint on the radio afterglow image size [34,89] but do not reveal its detailed surface brightness distribution, because of uncertainties in the scattering properties of the Galactic interstellar medium.)

The fireball of a GRB afterglow is predicted to appear on the sky as a ring (in the optical band) or a disk (at low radio frequencies) which expands laterally at a superluminal speed, $\sim \Gamma c$, where $\Gamma \gg 1$ is the Lorentz factor of the relativistic blast wave which emits the afterglow radiation [88,76,68,36]. For a spherical explosion into a constant density medium (such as the interstellar medium), the physical radius of the afterglow image is of order the fireball radius over Γ , or more precisely [36]

$$R_s = 3.9 \times 10^{16} \left(\frac{E_{52}}{n_1} \right)^{1/8} \left(\frac{t_{\text{days}}}{1+z} \right)^{5/8} \text{ cm}, \quad (2)$$

where E_{52} is the hydrodynamic energy output of the GRB explosion in units of 10^{52} ergs, n_1 is the ambient medium density in units of 1 cm^{-3} , and t_{days} is the

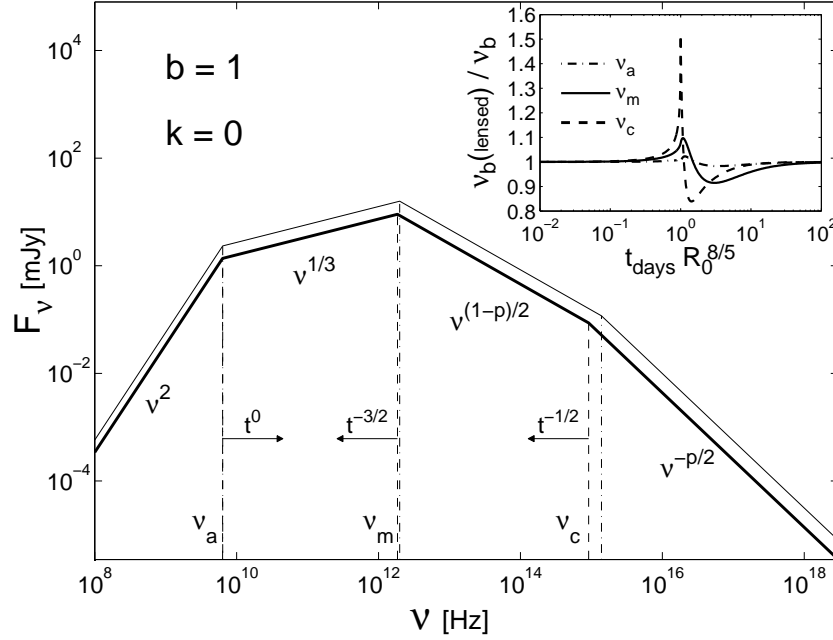


Fig. 4. A typical broken power-law spectrum of a GRB afterglow at a redshift $z = 1$ (from Granot & Loeb 2001). The observed flux density, F_ν , as a function of frequency, ν , is shown by the boldface solid line at an observed time $t_{\text{days}} = 1$ for an explosion with a total energy output of 10^{52} ergs in a uniform interstellar medium ($k = 0$) with a hydrogen density of 1 cm^{-3} , and post-shock energy fractions in accelerated electrons and magnetic field of $\epsilon_e = 0.1$ and $\epsilon_B = 0.03$, respectively. The thin solid line shows the same spectrum when it is microlensed by an intervening star with an impact parameter equal to the Einstein angle and $R_0 \equiv [\theta_s(1 \text{ day})/\theta_E] = 1$. The insert shows the excess evolution of the break frequencies $\nu_b = \nu_a$, ν_m and ν_c (normalized by their unlensed values) due to microlensing.

observed time in days. At a cosmological redshift z , this radius of the GRB image occupies an angle $\theta_s = R_s/D_A$, where $D_A(z)$ is the angular diameter distance at the GRB redshift, z . For the typical cosmological distance, $D_A \sim 10^{28} \text{ cm}$, the angular size is of order a micro-arcsecond (μas). Coincidentally, this image size is comparable to the Einstein angle of a solar mass lens at a cosmological distance,

$$\theta_E = \left(\frac{4GM_{\text{lens}}}{c^2 D} \right)^{1/2} = 1.6 \left(\frac{M_{\text{lens}}}{1M_\odot} \right)^{1/2} \left(\frac{D}{10^{28} \text{ cm}} \right)^{-1/2} \mu\text{as}, \quad (3)$$

where M_{lens} is the lens mass, and $D \equiv D_{\text{os}}D_{\text{ol}}/D_{\text{ls}}$ is the ratio of the angular-diameter distances between the observer and the source, the observer and the lens, and the lens and the source [77]. Loeb & Perna [57] showed that because

the ring expands laterally faster than the speed of light, the duration of the microlensing event is only a few days rather than tens of years, as is the case for more typical astrophysical sources which move at a few hundred km s^{-1} or $\sim 10^{-3}c$.

The microlensing lightcurve goes through three phases: (i) constant magnification at early times, when the source is much smaller than the source-lens angular separation; (ii) peak magnification when the ring-like image of the GRB first intersects the lens center on the sky; and (iii) fading magnification as the source expands to larger radii.

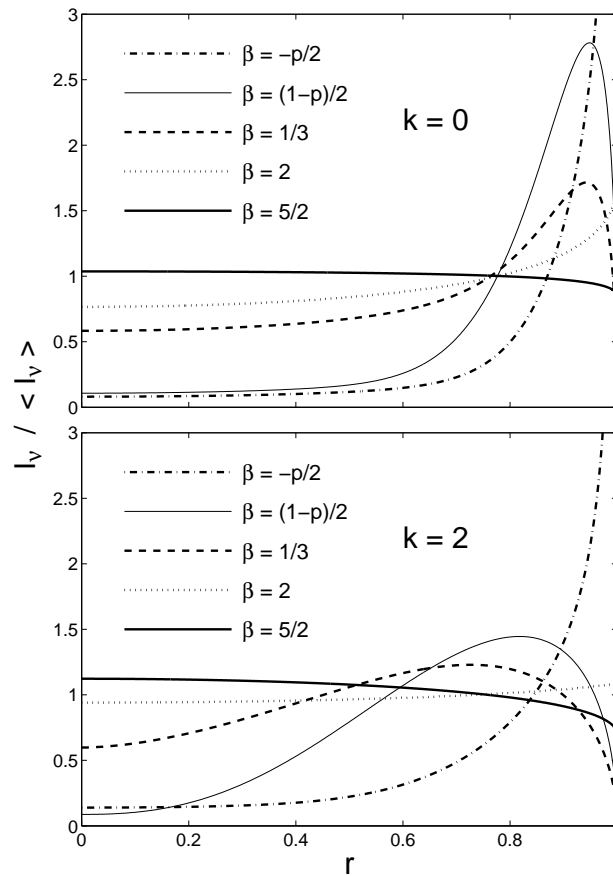


Fig. 5. The surface brightness, normalized by its average value, as a function of the normalized radius, r , from the center of a GRB afterglow image (where $r = 0$ at the center and $r = 1$ at the outer edge). The image profile changes considerably between different power-law segments of the afterglow spectrum, $F_\nu \propto \nu^\beta$ (see Figure 4). There is also a strong dependence on the power-law index of the radial density profile of the external medium around the source, $\rho \propto R^{-k}$ (taken from Granot & Loeb 2001).

Granot & Loeb [35] calculated the radial surface brightness profile (SBP) of the image of a Gamma-Ray-Burst (GRB) afterglow as a function of frequency and ambient medium properties, and inferred the corresponding magnification lightcurves due to microlensing by an intervening star. The afterglow spectrum consists of several power-law segments separated by breaks, as illustrated by Figure 4. The image profile changes considerably across each of the spectral breaks, as shown in Figure 5. It also depends on the power-law index, k , of the radial density profile of the ambient medium into which the GRB fireball propagates. Gaudi & Loeb [31] have shown that intensive monitoring of a microlensed afterglow lightcurve can be used to reconstruct the parameters of the fireball and its environment. The dependence of the afterglow image on frequency offers a fingerprint that can be used to identify a microlensing event and distinguish it from alternative interpretations. It can also be used to constrain the relativistic dynamics of the fireball and the properties of its gaseous environment. At the highest frequencies, the divergence of the surface brightness near the edge of the afterglow image ($r = 1$ in Figure 5) depends on the thickness of the emitting layer behind the relativistic shock front, which is affected by the length scale required for particle acceleration and magnetic field amplification behind the shock [60,37].

Ioka & Nakamura [44] considered the more complicated case where the explosion is collimated and centered around the viewing axis. More general orientations that violate circular symmetry need to be considered in the future.

GRB 000301C Garnavich, Loeb, & Stanek [29] have reported the possible detection of a microlensing magnification feature in the optical-infrared light curve of GRB 000301C (see Figure 6). The achromatic transient feature is well fitted by a microlensing event of a $0.5M_{\odot}$ lens separated by an Einstein angle from the source center, and resembles the prediction of Loeb & Perna [57] for a ring-like source image with a narrow fractional width ($\sim 10\%$). Alternative interpretations relate the transient achromatic brightening to a higher density clump into which the fireball propagates [5], or to a refreshment of the decelerating shock either by a shell which catches up with it from behind or by continuous energy injection from the source [91]. However, the microlensing model has a smaller number of free parameters. If with better data, a future event will show the generic temporal and spectral characteristics of a microlensing event, then these alternative interpretations will be much less viable. A galaxy $2''$ from GRB 000301C might be the host of the stellar lens, but current data provides only an upper-limit on its surface brightness at the GRB position. The existence of an intervening galaxy increases the probability for microlensing over that of a random line-of-sight.

Gaudi, Granot, & Loeb [32] have shown that direct inversion of the observed light curve for GRB 000301C yields a surface brightness profile (SBP) of the afterglow image which is strongly limb-brightened, as expected theoretically (see Figure 7).

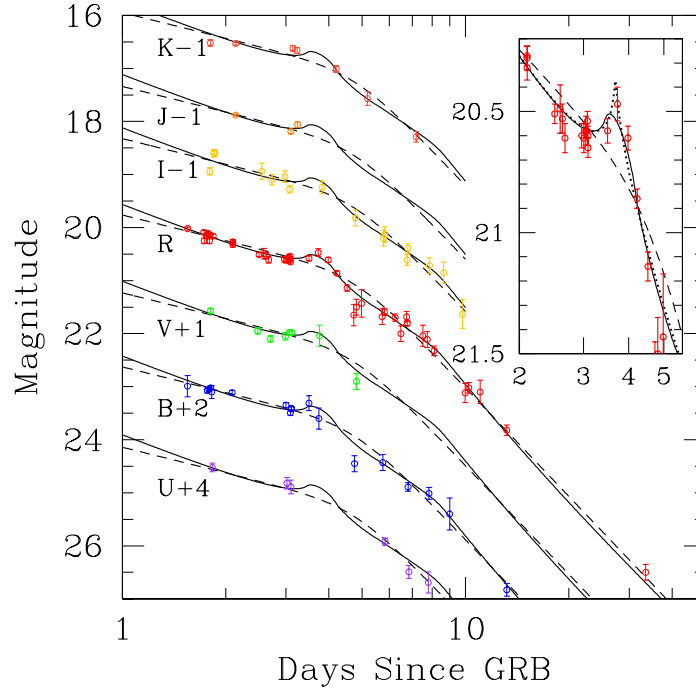


Fig. 6. *UBVRIJK* photometry of GRB 000301C as a function of time in days from the GRB trigger (from Garnavich et al. 2000; Gaudi et al. 2001). Data points have been offset by the indicated amount for clarity. The dashed line is the best-fit smooth, double power-law lightcurve (with no lensing), while the solid line is the overall best-fit microlensing model, where the SBP has been determined from direct inversion. The inset shows the *R*-band data only. The dotted line is the best-fit microlensing model with theoretically calculated SBP, for $k = 0$ and $\nu > \nu_c$.

Obviously, realistic lens systems could be more complicated due to the external shear of the host galaxy or a binary companion. Mao & Loeb [53] calculated the magnification light curves in these cases, and found that binary lenses may produce multiple peaks of magnification. They also demonstrated that *all* afterglows are likely to show variability at the level of a few percent about a year following the explosion, due to stars which are separated by tens of Einstein angles from the line-of-sight.

What is the probability for microlensing? If the lenses are not strongly clustered so that their cross-sections overlap on the sky, then the probability for having an intervening lens star at a projected angular separation θ from a source at a redshift $z \sim 2$ is $\sim 0.3\Omega_\star(\theta/\theta_E)^2$ [71,6,66,67], where Ω_\star is the cosmological density parameter of stars. The value of Ω_\star is bounded between the density of the luminous stars in galaxies and the total baryonic density as inferred from Big Bang nucleosynthesis, $7 \times 10^{-3} < \Omega_\star < 5 \times 10^{-2}$ [27]. Hence, *all* GRB af-

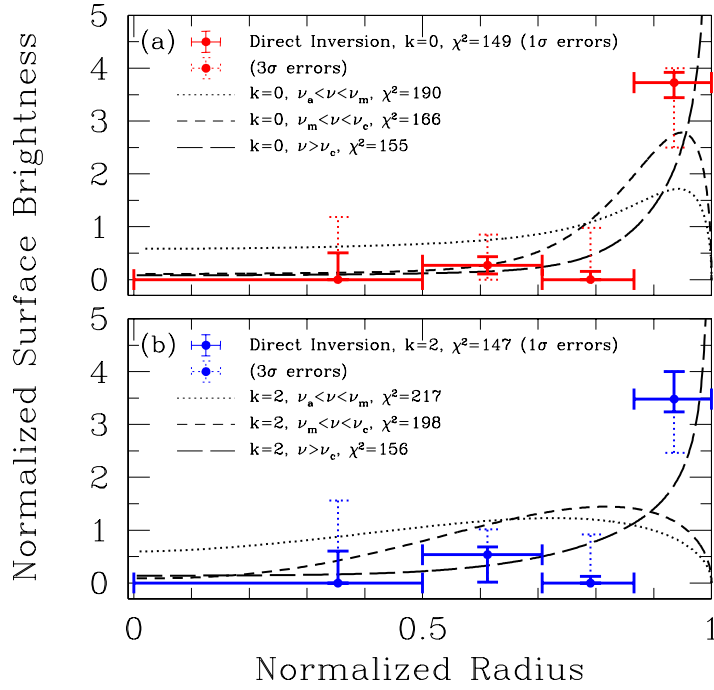


Fig. 7. Fitting GRB 000301C with different SBPs as a function of normalized radius (taken from Gaudi et al. 2001). The points are the SBPs determined from direct inversion, with 1σ errors (solid) and 3σ errors (dotted). The curves are theoretically calculated SBPs for various frequency regimes (see Figure 5). (a) Uniform external medium, $k = 0$. (b) Stellar wind environment, $k = 2$. The number of degrees of freedom is 92 for the direct inversion points and 89 for the curves.

terglows should show evidence for events with $\theta \sim 30\theta_E$, for which microlensing provides a small perturbation to the light curve[53]. (This crude estimate ignores the need to subtract those stars which are embedded in the dense central regions of galaxies, where macrolensing dominates and the microlensing optical depth is of order unity.) However, only one out of roughly a hundred afterglows is expected to be strongly microlensed with an impact parameter smaller than the Einstein angle. Indeed, Koopmans & Wambsganss [48] have found that the ‘a posteriori’ probability for the observed microlensing event of GRB 000301C along a random line-of-sight is between 0.7–2.7% if 20–100% of the dark matter is in compact objects.

Microlensing events are rare but precious. Detailed monitoring of a few strong microlensing events among the hundreds of afterglows detected per year by the forthcoming Swift satellite, could be used to constrain the environment and the

dynamics of relativistic GRB fireballs, as well as their magnetic structure and particle acceleration process.

2 Illumination of the Intergalactic Medium by Quasars

2.1 Ly α Halos

The absorption trough created in the spectrum of a distant sources due to neutral hydrogen diminishes down to undetectable flux levels as soon as the mean neutral fraction of hydrogen is larger than $\sim 10^{-4}$ (see equation 1). Once the transmitted flux reaches very low levels, it is difficult to infer whether the neutral fraction of hydrogen is as low as 0.01% or as high as 100%. A novel way to study the reionization phase transition relies on a direct detection of intergalactic neutral hydrogen. Loeb & Rybicki [58,75] have shown that the neutral gas prior to reionization can be probed through narrow-band imaging of embedded Ly α sources. The physical situation is analogous to the appearance of a halo of scattered light around a street lamp which is embedded in a dense fog. The “street lamp” in this metaphor is a high-redshift quasar which emits Ly α photons into the surrounding neutral hydrogen gas. The IGM scatters these photons and acts as a fog.

The radiation of the first galaxies is strongly absorbed shortward of their rest-frame Ly α wavelength by neutral hydrogen in the intervening IGM. However, the Ly α photons emitted by these sources are not eliminated but rather scatter until they redshift out of resonance and escape due to the Hubble expansion of the surrounding intergalactic hydrogen (see Fig. 8). Detection of the diffuse Ly α halos around high redshift sources would provide a unique tool for probing the neutral IGM before the epoch of reionization. Loeb & Rybicki [58,75] explored the above effect for a uniform, fully-neutral IGM in a pure Hubble flow. It is important to extend this analysis to more realistic cases of sources embedded in an inhomogeneous IGM, which is partially ionized by these sources [10]. It would be interesting to extract particular realizations of the perturbed IGM around massive galaxies from numerical simulations, and to apply a suitable radiative transfer code in propagating the Ly α photons from the embedded galaxies. Mapping of the properties of the associated Ly α halos will allow to assess their detectability with future observations.

2.2 Magnetization of the Intergalactic Medium by Quasar Outflows

Magnetic fields and cosmic rays play an important dynamical role in the interstellar medium of galaxies. However, they are often ignored in discussions of the intergalactic medium (IGM). *How significant is the pressure from these non-thermal components in the IGM? Has the magnetic field observed in collapsed objects, such as galaxies or clusters of galaxies, originated from the IGM?* The first question is particularly relevant for the reconstruction of the mass distribution of galaxy clusters from X-ray data.

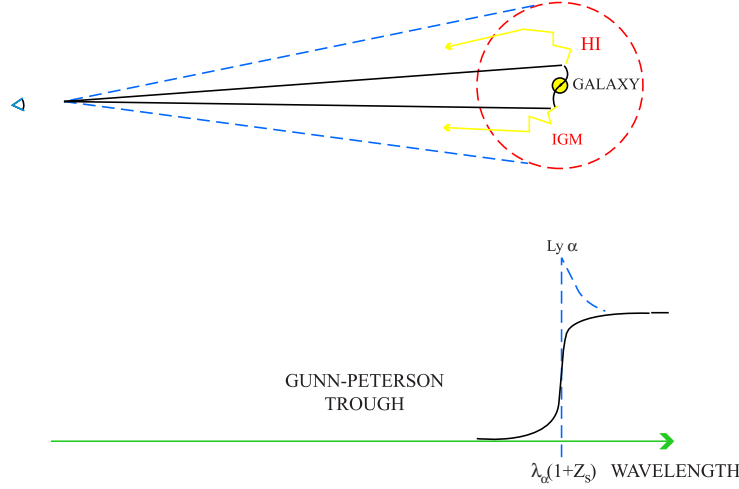
$\text{Ly}\alpha$ SOURCE BEFORE REIONIZATION


Fig. 8. *Loeb–Rybicki halos:* Scattering of $\text{Ly}\alpha$ line photons from a galaxy embedded in the neutral intergalactic medium prior to reionization. The line photons diffuse in frequency due to the Hubble expansion of the surrounding medium and eventually redshift out of resonance and escape to infinity. A distant observer sees a $\text{Ly}\alpha$ halo surrounding the source, along with a characteristically asymmetric line profile. The observed line should be broadened and redshifted by about one thousand km s^{-1} relative to other lines (such as $\text{H}\alpha$) emitted by the galaxy.

Outflows from quasars inevitably pollute the IGM with magnetic fields. The short-lived activity of a quasar leaves behind an expanding magnetized bubble in the IGM. Furlanetto & Loeb [28] modeled the expansion of the remnant quasar bubbles and calculated their distribution as a function of size and magnetic field strength at different redshifts. They have found that generically by a redshift $z \sim 3$, about 5–20% of the IGM volume is filled by magnetic fields with an energy density $> 10\%$ of the mean thermal energy density of a photo-ionized IGM at $\sim 10^4$ K (see Figure 9). As massive galaxies and X-ray clusters condense out of the magnetized IGM, the adiabatic compression of the magnetic field could result in the field strength observed in these systems without a need for further dynamo amplification. The intergalactic magnetic field could also provide a non-thermal contribution to the pressure of the photo-ionized gas that may account for the claimed discrepancy between the simulated and observed Doppler width distributions of the $\text{Ly}\alpha$ forest at $z > 2$ [11,83]. However, the supplied magnetic energy is unlikely to be dynamically important today since the present-day IGM was heated by gravitationally-induced shocks to an average mass-weighted temperature of $\sim 3 \times 10^6 \text{K}$ [13], larger by two orders of magnitude than the magnetic energy input from quasars.

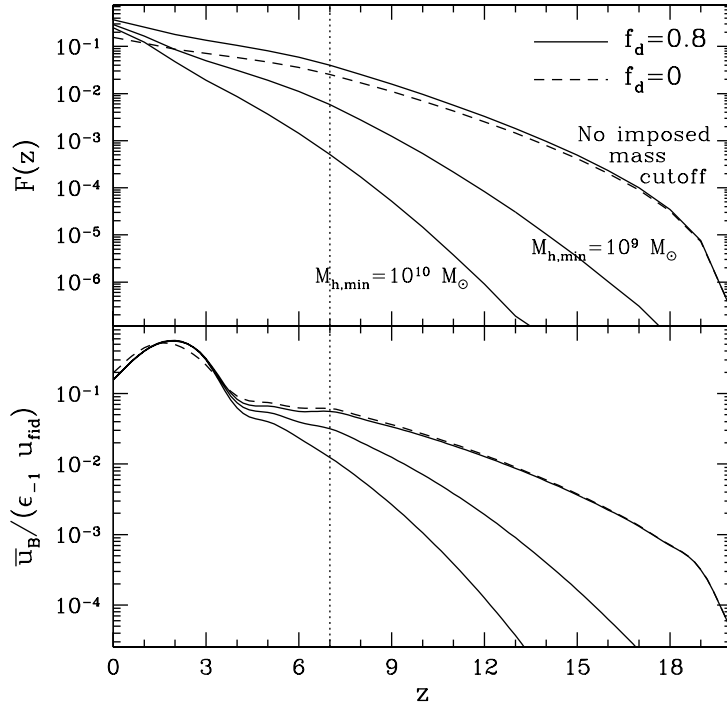


Fig. 9. *Upper Panel:* Volume filling fraction of magnetized bubbles $F(z)$, as a function of redshift (taken from Furlanetto & Loeb 2001). *Lower Panel:* Ratio of magnetic energy density, \bar{u}_B/ϵ_{-1} , to a fiducial thermal energy density $u_{fid} = 3n(z)kT_{IGM}$ of a photoionized IGM, where $T_{IGM} = 10^4$ K, as a function of redshift. The solid curves assume a different minimum mass for a galaxy out of which a quasar outflow may originate, $M_{h,min}$. Examples include a case where this minimum mass is determined by atomic cooling before reionization and by infall suppression afterward (top curve), and fixed-value cases with $M_{h,min} = 10^9 M_\odot$ (middle curve), and $M_{h,min} = 10^{10} M_\odot$ (bottom curve). The vertical dotted line indicates the assumed redshift of reionization, $z_r = 7$.

2.3 Particle Acceleration in Magnetized Intergalactic Shocks

Even though the present-day magnetic pressure may not be dynamically important, the magnetization of the IGM by quasar outflows has important consequences. Once magnetized, the shocks produced in the IGM during the formation of large-scale structure can accelerate a population of highly relativistic electrons by the Fermi mechanism, similarly to the collisionless shocks of supernova remnants. The accelerated electrons emit synchrotron radiation as they gyrate in the embedded magnetic fields and produce γ -ray radiation by inverse-Compton scattering the microwave background photons. This non-thermal radiation spans some ~ 20 orders of magnitude in photon energies from the radio to the TeV γ -ray regime. The radiation is expected to delineate the strong shocks formed

in the cosmic web of large scale sheets and filaments in the IGM. The brightest emission originates from the strongest intergalactic shocks around galaxy clusters.

2.4 Non-Thermal Radio and Gamma-Ray Emission

More than a third of all X-ray clusters with luminosities $> 10^{45} \text{ erg s}^{-1}$ possess diffuse radio halos [33]. Based on energy arguments and circumstantial evidence, these radio halos are believed to be caused by synchrotron emission from shock-accelerated electrons during the merger events of their host clusters ([41,86,21]; see [55] for references to alternative, less successful models). These highly-relativistic electrons cool primarily through inverse-Compton scattering off the microwave background. Since their cooling time is much shorter than the dynamical time of their host cluster, the radio emission is expected to last as long as the shock persists and continues to accelerate fresh electrons to relativistic energies. Intergalactic shocks also occur along the filaments and sheets that channel mass into the clusters. These structures, also traced by the galaxy distribution [16], are induced by gravity and form due to converging large-scale flows in the IGM.

The intergalactic synchrotron emission contaminates the cosmic microwave background (CMB) anisotropies – relic from the epoch of recombination, and as such needs to be considered in the design and analysis of anisotropy experiments at low frequencies. Previous estimates of synchrotron contamination of the cosmic anisotropies focused on Galactic emission, which occurs primarily at low Galactic latitudes and large angular scales [82]. Waxman & Loeb [90] calculated the intergalactic synchrotron contribution to the fluctuations in the radio sky as a function of frequency and angular scale (see Figure 10). They assumed that most of the emission originates from the virialization shocks around X-ray clusters, and used the Press–Schechter [72] mass function to describe the abundance of such clusters as a function of redshift (see also subsequent work in [26]). Although the synchrotron background amounts to only a small fraction of the CMB intensity, Waxman & Loeb [90] showed that its fluctuations could dominate over the primordial CMB fluctuations at low photon frequencies, $\nu < 10 \text{ GHz}$. They found that radio emission from cluster shocks contributes a fluctuation amplitude of $\sim 40 \mu\text{K} \times (\nu/10\text{GHz})^{-3}$ to the CMB on angular scales between 1 and 0.1° , respectively. Interestingly, current anisotropy experiments are just sensitive to this level of fluctuations. Existing detections by CAT ($50 \pm 15 \mu\text{K}$ at 15 GHz on $0.2\text{--}0.5^\circ$ scales) and OVRO ($56^{+8.5}_{-6.6} \mu\text{K}$ at 20 GHz on $0.1\text{--}0.6^\circ$ scales), as well as 95% upper limits ($< 40 \mu\text{K}$ on arcminute scales at $9\text{--}15 \text{ GHz}$ by the ATCA, RYLE and VLA detectors) are consistent with our prediction.

Loeb & Waxman [59] have shown that a significant fraction of the diffuse γ -ray background [78] might have been generated by the shocks resulting from the formation of large-scale structure in the intergalactic medium. Similarly to the collisionless shocks of supernova remnants [7], these shocks produce a population of highly-relativistic electrons with a maximum Lorentz factor $> 10^7$ that

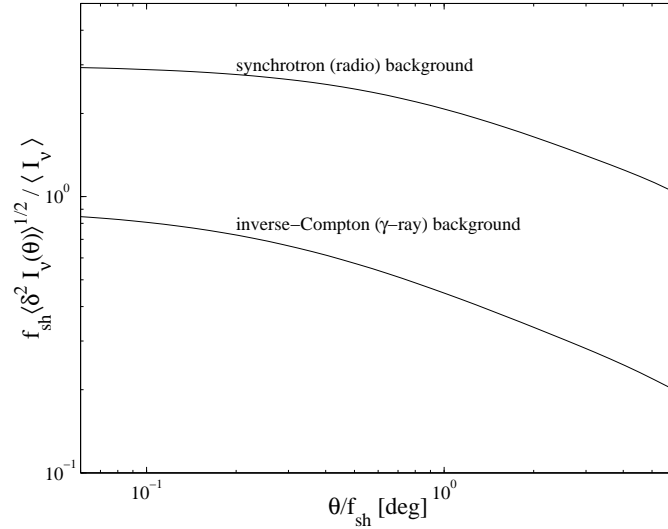


Fig. 10. Fractional intensity fluctuations, $(\langle I_\nu(0)I_\nu(\theta) \rangle - \langle I_\nu \rangle^2)^{1/2} / \langle I_\nu \rangle$, in synchrotron (radio) and inverse-Compton (γ -ray) background flux (taken from Waxman & Loeb 2000). The dimensionless coefficient, f_{sh} , is of order unity. The ratio of synchrotron to CMB intensity is $\langle I_\nu^{\text{syn}} \rangle / I_\nu^{\text{CMB}} = 6 \times 10^{-6} f_{\text{sh}}^{-2} (\xi_B / 0.01) (\nu / 10 \text{GHz})^{-3}$, where the post-shock magnetic energy fraction ξ_B is assumed to be of order 0.01, corresponding to a magnetic field strength of $0.1 \mu\text{G}$ in the virialization shock of X-ray clusters. The post-shock energy fraction carried by relativistic electrons is assumed to be $\xi_e \sim 0.05$, similar to the value inferred in the shocks of supernova remnants.

scatter a small fraction of the microwave background photons in the present-day universe up to γ -ray energies, thereby providing the γ -ray background. The predicted flux agrees with the observed diffuse background over more than four decades in photon energy and is not sensitive to the precise magnetic field value, provided that the fraction of shock energy carried by relativistic electrons is $\xi_e \sim 0.05$ (a value consistent with that inferred for supernovae shocks). The same electrons that emit γ -rays by inverse-Compton scattering of microwave background photons, also produce synchrotron radiation in the radio band due to intergalactic magnetic fields. The existence of magnetic fields with an amplitude $> 0.1 \mu\text{G}$, is inferred in cluster halos [47,30,74,45], and is also required for the Fermi acceleration of these electrons. The appearance of radio halos around young X-ray clusters is therefore a natural consequence and an important test of this model for the extragalactic γ -ray background. The combination of radio and γ -ray data can be used to calibrate ξ_e and determine the strength of the intergalactic magnetic field.

The assumed acceleration of electrons by collisionless shocks is similar to that observed in supernova remnants. Recent X-ray [49,50] and TeV [80,65] observations of the supernova remnants SN1006 and SNR RX J1713.7–3946 imply that electrons are accelerated in the remnant shocks up to an energy $\sim 100 \text{ TeV}$,

and are confined to the collisionless fluid by magnetic fields. These shocks have a velocity of order 10^3 km s^{-1} , similar to the velocity of the intergalactic shocks we consider here. Although the plasma density is very different in the two cases, the density may be scaled out of the problem by measuring time in units of ω_{pe}^{-1} , where ω_{pe} is the electron plasma frequency (shock characteristics may also depend on the pre-shock magnetic field, which introduces a dimensionless parameter into the problem, ω_{ce}/ω_{pe} , where ω_{ce} is the electron cyclotron frequency. However, for both supernova and IGM shocks, $\omega_{ce}/\omega_{pe} \ll 1$, suggesting a similar behavior in both cases). For supernova shocks, the inferred energy density in relativistic electrons constitutes 1–10% of the post-shock energy density in these remnants [18], a fraction consistent with the global ratio between the mean energy density of cosmic-ray electrons and the turbulent energy density in the interstellar medium of our galaxy.

The production of anisotropic backgrounds of radio and γ -ray radiation by strong intergalactic shocks is a natural consequence of structure formation in the Universe. The brightest emission originates from the shocks on Mpc scales around newly formed, massive X-ray clusters. The foreground synchrotron fluctuations might be comparable to the anisotropy signals detected by existing low-frequency microwave background experiments, and can be easily isolated through multi-frequency observations. Polarization anisotropy experiments could then constrain the coherence length of the intergalactic magnetic field.

Different astrophysical sources may contribute to the strength of the intergalactic magnetic fields; aside from radio sources [15,28] they include: the large scale shocks themselves [52], the first generation of stars [73] and supernova-driven winds from galaxies [51]. Different contributions may lead to different scalings of the magnetic field energy density with IGM gas parameters. The non-thermal γ -ray emission is only weakly dependent on the magnetic field strength [59]. However, the non-thermal radio emission is highly sensitive to this parameter and different models may lead to a different dependence of the radio emission on scale and redshift, which may have observable consequences (e.g. modifying the functional dependence of the correlation function shown in Figure 10).

Recent observations of the giant radio galaxy NGC 315 may constitute the first direct detection of collisionless large scale structure shocks, accelerating electrons to high energies [19]. Radio observations of this source are most naturally explained by the existence of a large scale shock produced by a flow converging towards an intersection of galaxy filaments [19].

Waxman & Loeb [90] predicted a fluctuation amplitude $> 40\%$ in the γ -ray background intensity on sub-degree scale, and the existence of extended, $> 1^\circ$, γ -ray halos, associated with newly formed massive clusters. On scales larger than a degree the fluctuation amplitude declines and is well below the anisotropy limits from EGRET (see Figure 5 in [78]). Detection of the predicted signals will provide a calibration of the uncertain model parameter, ξ_e . The high-energy maps required to detect the predicted anisotropy signal will be made between 20 MeV and 300 GeV by the GLAST instrument (planned for launch in 2005; see <http://glast.gsfc.nasa.gov/>), which is expected to be more sensitive than

EGRET by an order-of-magnitude [8]. The predicted γ -ray halos may constitute a significant fraction of the unidentified extra-Galactic EGRET sources [84,85]. However, since the angular extension of the brightest halos is large, a more careful analysis is required in order to assess the detectability of such halos by EGRET.

A future, dedicated, all-sky anisotropy experiment, operating at several frequencies below 10 GHz, would be able to map the fluctuations in the intergalactic synchrotron background. The resulting synchrotron map could then be cross-correlated with full-sky maps at hard X-ray or γ -ray energies to confirm its cosmic origin. Identification of the synchrotron fluctuations together with their counterpart inverse-Compton emission of hard X-rays or γ -rays by the same population of shock-accelerated electrons, can be used to empirically determine the strength and spatial distribution of the intergalactic magnetic field. Similarly, the correlation between radio and γ -ray halos may be detectable around individual X-ray clusters. Strong radio halos could be the best indicators for bright γ -ray clusters, which would provide the first obvious targets for GLAST.

Semi-analytic models [90] identify the intergalactic shocks with smooth spherical accretion of gas onto clusters, while in reality they result from asymmetric mergers as well as from converging flows in large scale sheets and filaments. The more realistic emission from these complex geometries can be best modeled through detailed hydrodynamic simulations [61,63,46]. Mergers of comparable mass clusters, for example, would tend to produce only mild shocks due to the prior heating of the shocked gas, leading to reduced non-thermal emission due to the steep power-law slope of the accelerated electrons.

In analogy with the collisionless shocks of supernova remnants, the intergalactic shocks are also expected to accelerate a hadronic cosmic-ray component that would acquire a fraction (~ 10 –50%) of the post-shock energy more substantial than that carried by relativistic electrons (~ 1 –10%, see [18]). Collisions of the hadronic cosmic-rays with IGM protons produce pions, π^0 , which decay into γ -ray photons; however for typical parameters this radiation component is expected to be sub-dominant relative to the inverse-Compton production of γ -rays by the relativistic electrons [59,90,62]. The buoyancy of the relativistic cosmic-ray fluid may lead to instabilities that would eventually separate it from the IGM gas and allow it to expand into the large-scale voids that fill most of the volume in between the sheets and filaments of the IGM. For a relativistic fluid, the adiabatic decrease of the pressure with increasing volume ($p \propto V^{-4/3}$) is milder than for the IGM gas ($p \propto V^{-5/3}$). It is possible that the intergalactic voids are currently being dominated by cosmic-ray and magnetic field pressure which suppresses the formation of galaxies there.

Acknowledgements

I thank all my collaborators on the topics described in this brief review: Rennan Barkana, Benedetta Ciardi, Steve Furlanetto, Peter Garnavitch, Scott Gaudi, Jonathan Granot, Zoltan Haiman, Shude Mao, Rosalba Perna, George Rybicki, Kris Stanek, and Eli Waxman. This work was supported in part by NASA grants NAG 5-7039, 5-7768, and by NSF grants AST-9900877, AST-0071019.

References

1. T. Abel, G. Bryan, M. L. Norman: *Ap. J.*, **540**, 39 (2000)
2. A. I. Anderson, et al.: *A. & A.*, **364**, L54 (2000)
3. R. Barkana, A. Loeb: *Physics Reports*, **349**, 125 (2001)
4. R. H. Becker et al: *Astr. J.*, **submitted**; astro-ph/0108097 (2001)
5. E. Berger, et al.: *Ap. J.*, **545**, 56 (2000)
6. O. M. Blaes, R. L. Webster: *Ap. J.*, **391**, L63 (1992)
7. R. Blandford, D. Eichler: *Physics Reports*, **154**, 1 (1987)
8. E. D. Bloom: *Space Sci. Rev.*, **75**, 109 (1996)
9. V. Bromm, P. S. Coppi, R. B. Larson: **527**, 5 (1999)
10. V. Bromm, A. Loeb, G. Rybicki: in preparation (2001)
11. G.L. Bryan, M. Machacek, P. Anninos, M.L. Norman: *Ap. J.*, **517**, 13 (1999)
12. B. Ciardi, A. Loeb: *Ap. J.*, **540**, 687 (2000)
13. R. Dave, et al.: *Ap. J.*, **552**, 473 (2001)
14. S. G. Djorgovski, S. M. Castro, D. Stern, A. Mahabal: *Ap. J. L.*, **submitted**; astro-ph/0108069 (2001)
15. R. A. Daly, A. Loeb: *Ap. J.* **364**, 451 (1990)
16. A. G. Doroshkevich et al.: *M.N.R.A.S.*, **283**, 1281 (1996)
17. S. L. Ellison, A. Songaila, J. Schaye, M. Pettini: *A. J.*, **120**, 1175 (2000)
18. D. C. Ellison, P. Slane, B. M. Gaensler: *Ap. J.*, **submitted**; astro-ph/0106257 (2001)
19. T. A. Ensslin et al.: *Ap. J.*, **549**, L39 (2001)
20. X. Fan, et al.: *A. J.*, **120**, 1167 (2000)
21. L. Feretti: to appear in *Proc. of IAU Symp. # 199* on “The Universe at Low Radio Frequencies”, Pune, India; astro-ph/0006379 (2000)
22. F. Fiore, F. Nicastro, S. Savaglio, L. Stella, M. Vietri: *Ap. J.*, **544**, L7 (2000)
23. D. A. Frail, et al.: *Nature*, **submitted** (2001); astro-ph/0102282
24. D. L. Freedman, E. Waxman: *Ap. J.*, **547**, 922 (2001)
25. A. Fruchter: *Ap. J.*, **512**, L1 (1999)
26. Y. Fujita, C. L. Sarazin, *Ap. J.*, **in press**; astro-ph/0108369 (2001)
27. M. Fukugita, C. J. Hogan, P. J. E. Peebles: *Nature*, **366**, 309 (1998)
28. S. R. Furlanetto, A. Loeb: *Ap. J.*, **556**, 619 (2001)
29. P. M. Garnavich, A. Loeb, K. Z. Stanek: *Ap. J.*, **544**, L11 (2000)
30. R. Fusco-Femiano et al.: *Ap. J.*, **513**, L21 (1999)
31. B. S. Gaudi, A. Loeb: *Ap. J.*, **558** (2001)
32. B. S. Gaudi, J. Granot, A. Loeb: *Ap. J.*, **in press** (2001)
33. G. Giovannini, M. Tordi, L. Feretti: *New Astronomy*, **4**, 141 (1999)
34. J. Goodman: *New Astronomy*, **2**, 449 (1997)
35. J. Granot, A. Loeb: *Ap. J.*, **551**, L63 (2001)
36. J. Granot, T. Piran, R. Sari: *Ap. J.*, **513**, 679 (1999a); **527**, 236 (1999b)
37. A. Gruzinov, E. Waxman: *Ap. J.*, **511**, 852 (1999)
38. J. E. Gunn, B. A. Peterson: *Ap. J.*, **142**, 1633, (1965)
39. Z. Haiman, A. Loeb: *Ap. J.*, **483**, 21 (1997); **503**, 505 (1998); **552**, 459 (2001)
40. F. Hamann, G. Ferland: *A. R. A. & A.* **37**, 487 (1999)
41. D. E. Harris, V. K. Kapahi, R. D. Ekers: *Astr. &Ap. Suppl.*, **39**, 215 (1995)
42. F. D. A. Hartwick, D. Schade: *A. R. A. & A.*, **28**, 437 (1990)
43. U. Hellsten, N. Y. Gnedin, J. Miralda-Escude: *ApJ*, **509**, 56 (1998)
44. K. Ioka, K., T. Nakamura: *Ap. J.*, **in press**; astro-ph/0102028 (2001)
45. J. S. Kaastra, et al.: *Ap. J.*, **519**, L119 (1999)

46. U. Keshet, E. Waxman, V. Springel, A. Loeb, L. Hernquist: *Ap. J.*, in preparation (2001)
47. K.-T. Kim, P. P. Kronberg, G. Giovannini, T. Venturi: *Nature*, **341**, 720 (1989)
48. L. V. E. Koopmans, J. Wambsganss: *M.N.R.A.S.*, **in press**; astro-ph/0011029 (2001)
49. K. Koyama et al.: *Nature*, **378**, 255 (1995)
50. K. Koyama et al.: *PSAJ*, **49**, L7 (1997)
51. P. P. Kronberg, H. Lesch, U. Hopp: *Ap. J.*, **511**, 56 (1999)
52. R. M. Kulsrud, R. Cen, J. P. Ostriker, D. Ryu: *Ap. J.*, **454**, 60 (1997)
53. S. Mao, A. Loeb: *Ap. J.*, **547**, L97 (2001)
54. D. Q. Lamb, D. E. Reichart: *Ap. J.* **536**, 1 (2000)
55. H. Liang, R. W. Hunstead, M. Birkinshaw, P. Andreani: *Ap. J.*, **544**, 686 (2000)
56. A. Loeb, R. Barkana: *ARA&A*, **in press** (2001)
57. A. Loeb, R. Perna: *Ap. J.*, **495**, 597 (1998)
58. A. Loeb, & G. Rybicki: *Ap. J.*, **524**, 527 (1999)
59. A. Loeb, E. Waxman: *Nature*, **405**, 156 (2000)
60. M. V. Medvedev, A. Loeb: *Ap. J.* **526**, 697 (1999)
61. F. Miniati, D. Ryu, H. Kang, T. W. Jones, R. Cen, J. P. Ostriker: *Ap. J.*, **542**, 608 (2000)
62. F. Miniati, D. Ryu, H. Kang, T. W. Jones: *Ap. J.*, **559**, 1 (2001)
63. F. Miniati, T. W. Jones, H. Kang, D. Ryu: *Ap. J.*, **in press**; astro-ph/0108305 (2001)
64. J. Miralda-Escudé: *Ap. J.*, **501**, 15 (1998)
65. H. Muraishi et al.: *Astr. & Ap.*, **354**, L57 (2000)
66. R. Nemiroff: *Ap.& SS*, **259**, 309 (1998)
67. R. Nemiroff, J. P. Norris, J. T. Bonnell, G. F. Marani: *Ap. J.*, **494**, L173 (1998)
68. A. Panaitescu, P. Mészáros: *Ap. J.*, **493**, L31 (1998)
69. R. Perna, A. Loeb: *Ap. J.*, **501**, 467 (1998)
70. R. Perna, & A. Loeb: *Ap. J.*, **503**, L135 (1998)
71. W. H. Press, J. E. Gunn: *Ap. J.*, **185**, 397 (1973)
72. W. H. Press, P. Schechter: *Ap. J.*, **187**, 425 (1974)
73. M. J. Rees: *QJRAS*, **28**, 197 (1987)
74. Y. Rephaeli, D. Gruber, P. Blanco: *Ap. J.*, **511**, L21 (1999)
75. G. Rybicki, & A. Loeb: *Ap. J.*, **520**, L79 (1999)
76. R. Sari: *Ap. J.*, **494**, L49 (1998)
77. P. Schneider, J. Ehlers, E. E. Falco: *Gravitational Lenses* (Springer, Heidelberg 1992)
78. P. Sreekumar et al.: *Ap. J.*, **494**, 523 (1998)
79. D. Stern, H. Spinrad: *P. A. S. P.*, **111**, 1475 (1999)
80. T. Tanimori et al.: *Ap. J.*, **497**, L25 (1998)
81. M. Tegmark, J. Silk, A. Evrard: *Ap. J.*, **417**, 54 (1993)
82. M. Tegmark, D.J. Eisenstein, W. Hu, A. de Oliveira-Costa: *Ap. J.*, **530**, 133 (2000)
83. T. Theuns, A. Leonard, G. Efstathiou, F.R. Pearce, P.R. Thomas: *M.N.R.A.S.*, **301**, 478 (1998)
84. T. Totani, T. Kitayama: *Ap. J.*, **545**, 572 (2000)
85. W. Kawasaki, T. Totani: *Ap. J.*, **submitted**; astro-ph/0108309 (2001)
86. P. Tribble: *M.N.R.A.S.*, **263**, 31 (1993)
87. X. Wang, M. Tegmark, M. Zaldarriaga: *Phys. Rev. D*, **submitted**; astro-ph/0105091 (2001)
88. E. Waxman: *Ap. J.*, **491**, L19 (1997)
89. E. Waxman, S. R. Kulkrani, D. A. Frail: *Ap. J.*, **497**, 288 (1998)
90. E. Waxman, A. Loeb: *Ap. J.*, **545**, L11 (2000)
91. Z. Zhang, P. Meszaros: *Ap. J.*, **552**, L35 (2001)